

Noise Source Identification with Increased Spatial Resolution

Svend Gade, Jørgen Hald and Bernard Ginn

Brüel & Kjær Sound & Vibration Measurements A/S, Nærum, Denmark

Delay-and-sum (DAS) planar beamforming has been a widely used noise-source identification technique for the last decade. It is a quick one-shot measurement technique to map sources that are larger than the array itself. The spatial resolution is proportional to distance between array and source and inversely proportional to wavelength, so the resolution is only good at medium to high frequencies. Improved algorithms using iterative de-convolution techniques offer up to 10 times better resolution. The principle behind these techniques is described here along with measurement examples from various industries.

Beamforming is an array-based measurement technique for sound-source location from medium to long measurement distances. Basically, the source location is performed by estimating the amplitudes of plane (or spherical) waves incident toward the array from a chosen set of directions. The angular resolution is inversely proportional to the array diameter measured in units of wavelength, so the array should be much larger than the wavelength to get a fine angular resolution. At low frequencies, this requirement usually cannot be met, so here the resolution will be poor.

For typical, irregular array designs, the beamforming method does not allow the measurement distance to be much smaller than the array diameter. On the other hand, the measurement distance should be kept as small as possible to achieve the finest possible resolution on the source surface. Of course, this is not possible when measuring large objects. The use of a discrete set of measurement points on a plane can be seen as a spatial sampling of the sound field. Near-field acoustical holography, NAH as well as SONAH (statistically optimized NAH) require a grid spacing less than half a wavelength at the highest frequency of interest.³ At higher frequencies the number of measurement points gets very high. When the grid spacing exceeds half a wavelength, spatial aliasing components or interpolation errors quickly get very disturbing.

On the other hand, irregular arrays can potentially provide a much smoother transition – spatial aliasing effects can be kept at an acceptable level up to a much higher frequency with the same average spatial sampling density. This indicates why beamforming can measure up to high frequencies and provide a good resolution with a fairly low number of microphones. So beamforming is an attractive alternative and supplement to NAH/SONAH, because measurements can be taken at some intermediate distance with a highly sparse array, which is not required to be larger than the noise source. And at high frequencies, beamforming can provide quite good resolution.

Theory of Beamforming

As illustrated in Figure 1, we consider a planar array of M microphones at M distributed locations r_m ($m=1,2,\dots,M$) in the x - y plane of our coordinate system. When such an array is applied for, delay-and-sum beamforming, the measured pressure signals p_m are individually delayed and then summed:^{1,2}

$$b(\kappa, t) = \sum_{m=1}^M p_m(t - \Delta_m(\kappa)) \quad (1)$$

The individual time delays Δ_m are chosen with the aim of achieving selective directional sensitivity in a specific direction, characterized here by a unit vector κ . This objective is met by adjusting the time delays in a way that signals associated with a plane wave, incident from the direction κ , will be aligned in time before they are summed. Geometrical considerations (see Figure 1) show that this can be obtained by choosing:

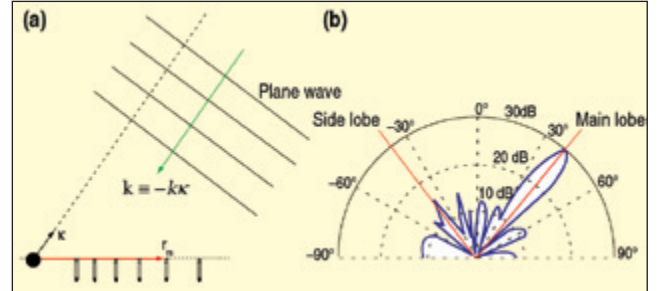


Figure 1. (a) Microphone array, a far-field focus direction, and a plane wave incident from the focus direction; (b) Directional sensitivity diagram with main lobe in the focus direction and lower side lobes in other directions.

$$\Delta_m = \frac{\kappa \cdot r_m}{c} \quad (2)$$

where c is the propagation speed of sound. Signals arriving from other far-field directions will not be aligned before the summation, so they will not coherently add up.

The frequency domain version of Equation 1 for the delay-and-sum beamformer output is:

$$B(\kappa, \omega) = \sum_{m=1}^M P_m(\omega) e^{-j\omega \Delta_m(\kappa)} = \sum_{m=1}^M P_m(\omega) e^{j\kappa \cdot r_m} \quad (3)$$

Here, ω is the temporal angular frequency; $\mathbf{k} = -\kappa \kappa$ is the wave number vector of a plane wave incident from the direction κ in which the array is focused (see Figure 1); and $k = \omega/c$ is the wave number. In Equation 3, an implicit time factor equal to $e^{j\omega t}$ is assumed.

The frequency domain beamformer will have a “main lobe” of high directional sensitivity around the focus direction and lower sensitivity in other directions, although with some lower “side lobes” (see Figure 1b). The width of the main lobe can be shown to define an on-axis angular resolution equal to λ/D , where λ is wavelength, and D is the diameter of the array. At a measurement distance equal to L , this angular resolution corresponds to a spatial resolution, R , given by the expression:

$$R = \frac{L}{D} \lambda \quad (4)$$

The measurement distance, L , should not be much smaller than the array diameter, D . For comparison, NAH provides a resolution around $\lambda/2$ at high frequencies and approximately equal to L at lower frequencies. At low frequencies, therefore, NAH can provide significantly better resolution when a sufficiently small measurement distance is used.

Beamforming with Increased Spatial Resolution

Using iterative de-convolution techniques, it is possible to achieve higher resolution than provided by standard DAS beamforming techniques.⁴ The idea is that when measuring a point source, the DAS beamforming pressure power result is given by the location of the point source convolved by the beamformer’s directional characteristics, as shown in Figure 1b and produces what is known as the point-spread function (PSF).

For a given beamformer array, this PSF is known and can be compensated by using de-convolution techniques. This de-convolution gives a possibility to increase the spatial resolution of acoustic arrays and reduce disturbing side lobe effects. In many fields of imaging, like for example optical and radio astronomy, de-convolution methods are widely used to increase the spatial resolution. For that

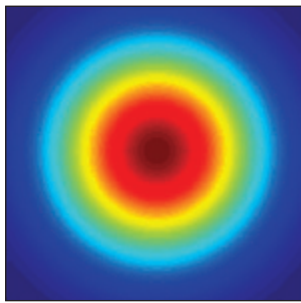


Figure 2. Point-spread function for an on-axis monopole at the focus plane.

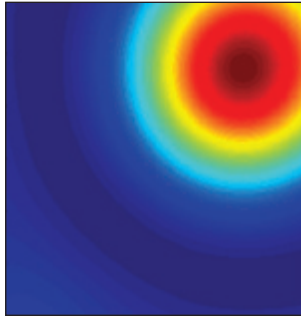


Figure 3. Point-spread function for a slightly off-axis monopole at the focus plane.

purpose a variety of algorithms has been developed in the past – for example, non-negative least-squares (NNLS) algorithm.

In recent years, these algorithms have been applied to acoustic array measurements, and some of the most promising ones are the fast spatial FFT-based de-convolution approach for mapping acoustic sources, version 2 (or DAMAS2) and the FFT-NNLS. From a practical point of view there are only minor differences between the two approaches, except that FFT-NNLS is a little slower but often more precise than DAMAS2.

The steps of the algorithms can be visualized – for a given array design, monopoles are placed at a grid of positions covering the mapping area on the source plane. For each monopole position i a DAS beamforming measurement is simulated, and the pressure power distribution on the source plane is calculated. Therefore, the PSF_i , which only depends on the test geometry, is obtained for each source location, i . Two examples are shown in Figures 2 and 3.

For the actual array measurement, an incoherent point-source model is used, and a solution is found in a least-squares sense for non-negative monopole power strengths, i.e. $A_i \geq 0$ (see Figure 4).

The output from DAS is smeared by the individual PSF_i . As an approximation, a position-independent point-spread function (shift invariant across the mapping area) is assumed, so the one at the center of the mapping area PSF_0 is used in Equation 5. Here, $A = \{A_i\}$ is a matrix containing all the source strengths, and the symbol \otimes represents convolution in x and y . Finally Equation 5 is solved iteratively for A (de-convolution), which means that in practice, the spatial resolution is improved compared to the original DAS by a factor 3-10, depending on the geometry of the array and test object. In practice approximately 50-100 iteration steps are enough.

$$DAS \approx A \otimes PSF_0 \quad \text{with} \quad A = \{A_i\} \quad \text{and} \quad A_i \geq 0 \quad (5)$$

Figure 5 shows the beamforming results from a side mirror in a wind tunnel with a wind speed of 80 mph, yaw angle of -20° , frequency of 992 Hz, bandwidth of 16 Hz and a display range of 6 dB for various iterations using the FFT-NNLS algorithm. Zero iterations correspond to an ordinary delay-and-sum beamforming. The car in the wind tunnel is shown in Figure 6.

Noise Measurements from Automotive Wind Tunnels

For beamforming measurements in wind tunnels, it is usual to place a half wheel on the floor of the tunnel to take advantage of the mirror ground condition. As the array is usually a few meters from the vehicle under test, it is also well outside the air flow region, so wind-induced noise is reduced. All the cross-spectra are measured simultaneously, which enables the wind noise induced in the microphones to be suppressed by using only the cross terms in the complete cross-spectrum matrix. The autospectra on the diagonal of this matrix are not used in the further calculation; this improves the S/N ratio. No microphone references are necessary.

Figure 6 shows a vehicle in a wind tunnel, where the sound distribution was investigated as a function of yaw angle. The vehicle was fully taped to reduce the effects of leakage around seals and to reduce turbulence produced by wheel arches, undercarriage, etc.⁵

Using a reference signal from, for example, a microphone positioned in the cabin close to the side mirror, effectively produces a selective beamformer; the noise from around the mirror and A-

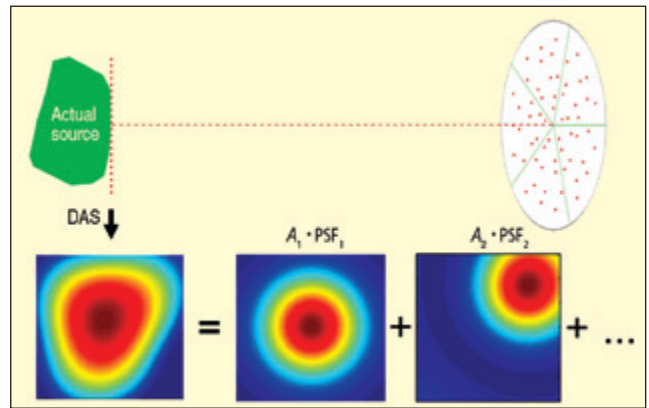


Figure 4. Incoherent source model is found in a least-squares sense.

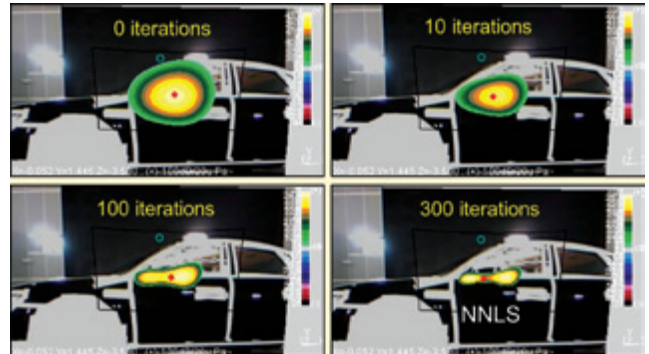


Figure 5. FFT-NNLS de-convolution beamforming results using different number of iterations.



Figure 6. Wind tunnel with taped vehicle on rotating plate used to adjust yaw angle; spherical beamformer in the cabin and half-wheel beamforming array at 3.8 m distance (0 degree yaw).

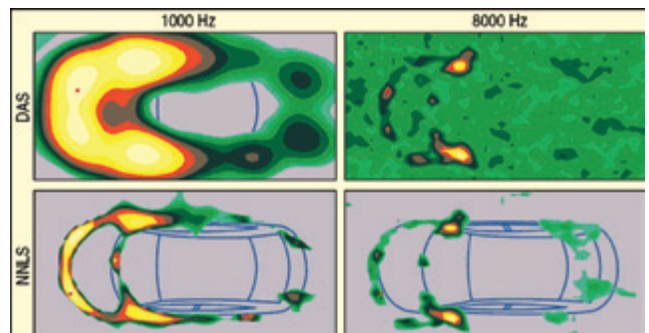


Figure 7. Wheel array supported above test vehicle in wind tunnel; 15-dB display range; NNLS yields better resolution at all frequencies and better suppression of side lobes at higher frequencies.

pillar will be accentuated, while the noise contribution from the turbulence produced by the front of the vehicle will be suppressed.

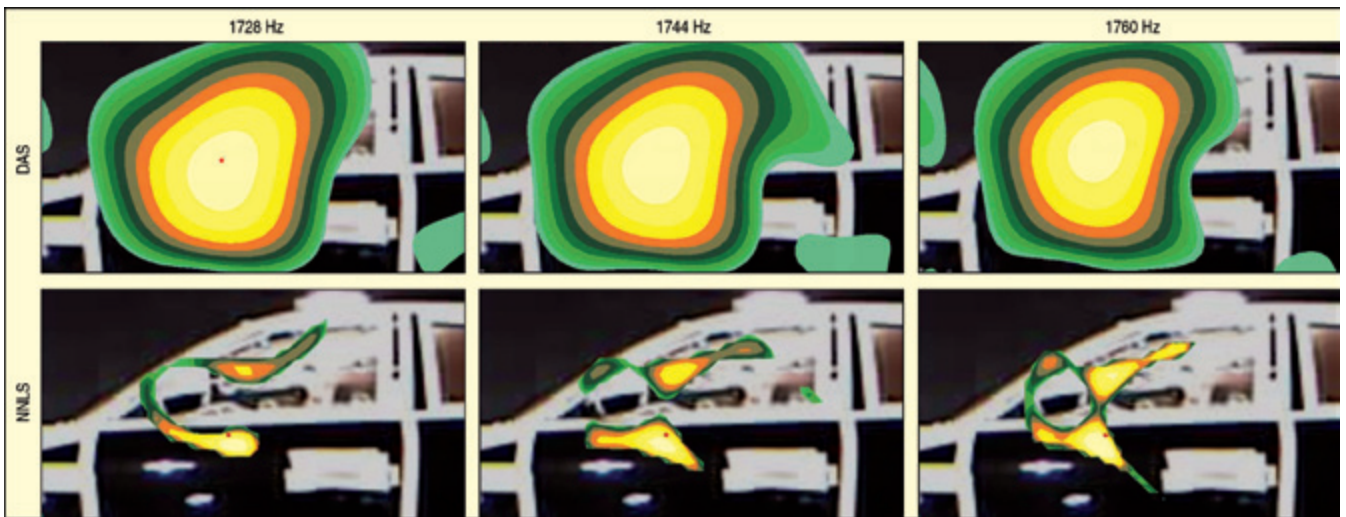


Figure 8. Low-intrusion A-pillar and side mirror at -10° yaw; 10 dB display range.

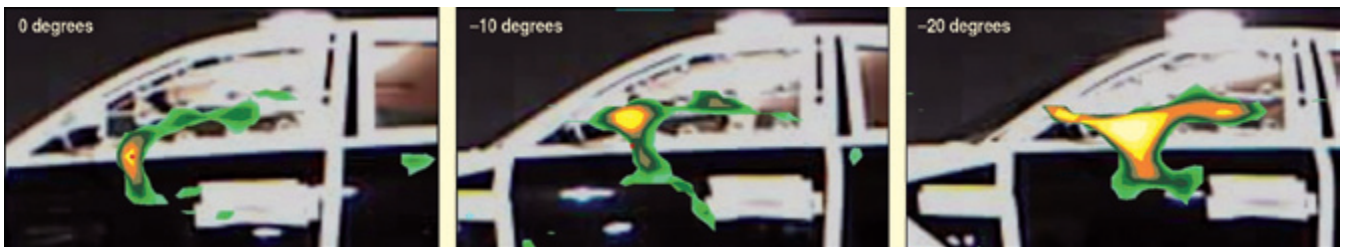


Figure 9. Non-negative least-squares (NNLS) results for various angles of yaw, frequency range 1784 to 1848 Hz; front of vehicle progressively turned toward half-wheel array; 10-d B display range.



Figure 10. Pentangle array for field measurement of large structures and for moving noise sources.

The main sources of aerodynamic noise perceived by the driver are usually the A-pillar and the side mirror. Therefore, exterior beamforming focuses on these areas. Figure 7 shows results using a full-wheel beamforming array hung above the roof of a vehicle.

The results were calculated for two different beamforming algo-

rithms. DAS is the most commonly used beamforming algorithm. While NNLS is a de-convolution method well known in other industries, as noted earlier. As clearly seen in Figure 7, NNLS offers better resolution at lower frequencies and better suppression of side lobes at higher frequencies compared with DAS.

In Figure 8, sound maps around the A-pillar and side mirror are shown for noise in 16-Hz bandwidths. Virtually no difference is noticed for the DAS results, while the NNLS shows considerable frequency-related detail.

In Figure 9, as the yaw angle of the vehicle is increased from 0° to 10° to 20° , one can see that on the leeward side, the amount of turbulent noise produced gradually increases.

Noise Measurements of Moving Sources

The first moving source measurement example is from the wind turbine industry. Here, simple DAS beamforming and de-convolution beamforming has been applied to the measurement data. A pentangular array with a diameter of 3.5 m, consisting of 5 arms with a total of 30 microphones has been used (see Figure 10). The horizontal distance to the tower was 38 m (also approximately the height of the wind turbine), and the array was tilted at an angle of 45° .

Also, it is clear in this case that de-convolution beamforming offers better resolution at most frequencies and better dynamic range at high frequencies (see Figure 11). The results here are shown for upwind measurement, while the corresponding downwind measurements clearly revealed the nacelle as a major noise source. The wings are moving clockwise in the picture, so it is also seen that most noise radiation toward the array position takes place when the wings are moving downward toward the ground.

The last example is from fly-over measurements where all features of refined beamforming had been used (combination of de-convolution, array shading, diagonal auto-spectra removal and source tracking). Aircraft position during a fly-over is measured with an onboard GPS system together with speed, roll, yaw and pitch. Synchronization with array data is achieved through recording of an IRIG-B time-stamp signal together with the array data and also with the GPS data on the aircraft.

The beamforming calculation is performed with a standard,

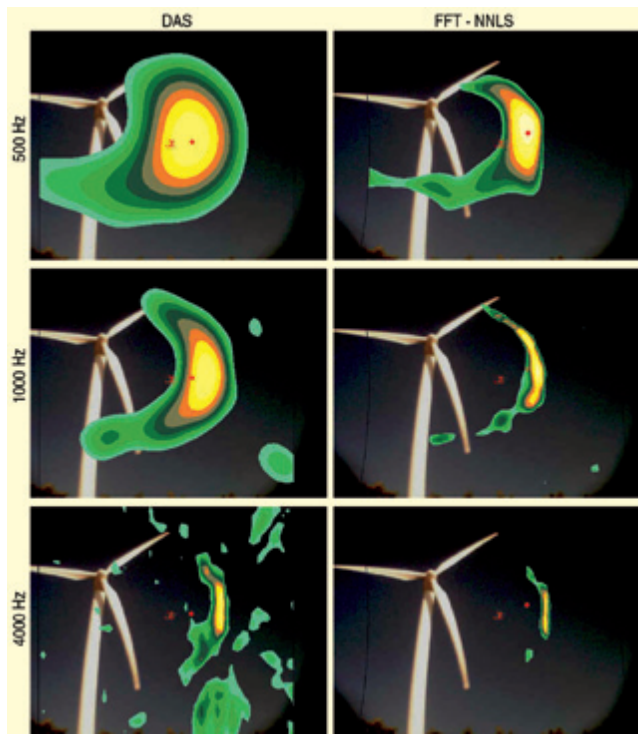


Figure 11. Delay-and-sum (DAS) beamforming results compared to deconvolution results from wind turbine measurements for 500 Hz, 1000 Hz and 4000 Hz one-third octave bands respectively.

tracking, time-domain DAS algorithm. For each focus point in the moving system, FFT and averaging in short time intervals is then performed to obtain spectral noise source maps representing the aircraft positions at the middle of the averaging intervals. Diagonal removal is implemented as described in Reference 1, providing the capability of suppressing contributions to the averaged spectra from the wind noise output of the individual microphones.

With sufficiently short averaging intervals, the array beam pattern will remain almost constant during the corresponding sweep of each focus point. This means that a de-convolution calculation can be performed for each FFT frequency line and for each averaging interval to enhance resolution, suppress side lobes and scale the maps.⁶

Figure 12 shows the array geometry and a picture of the array deployed on the runway. The array design and the use of a frequency-dependent, smooth, array-shading function was applied. (That is, the radius of the part of the array used for calculation is inversely proportional to frequency or proportional to wavelength, which means that the beamforming resolution will be frequency independent over the frequency range used).

However, to support quick and precise deployment on the runway, a simple star-shaped array geometry was implemented. The full array consists of nine identical line arrays that are joined together at a center plate, with equal angular spacing controlled by aluminum arcs. The 12 microphones on one line array six meters long were mounted into an aluminum tube that was rotated around its axis so that the 1/4-inch microphones were touching the runway. The surface geometry of that part of the runway, where the array was deployed, was very smooth and regular, so it could be characterized to a sufficient accuracy by just measuring a few slope parameters. So measurement of individual microphone coordinates was not necessary; the vertical positions were automatically and accurately obtained from the known microphone coordinates in the horizontal plane and the runway slopes.

About 120 measurements were taken on an MU300 business jet from Mitsubishi Heavy Industries, which has overall length and width equal to 14.8 m and 13.3 m, respectively. It has two jet engines on the body, just behind and over the wings. Most of the measurements were taken at an altitude of approximately 60 m and a speed of about 60 m/s (≈ 220 km/h).

A very big improvement in resolution and dynamic range was

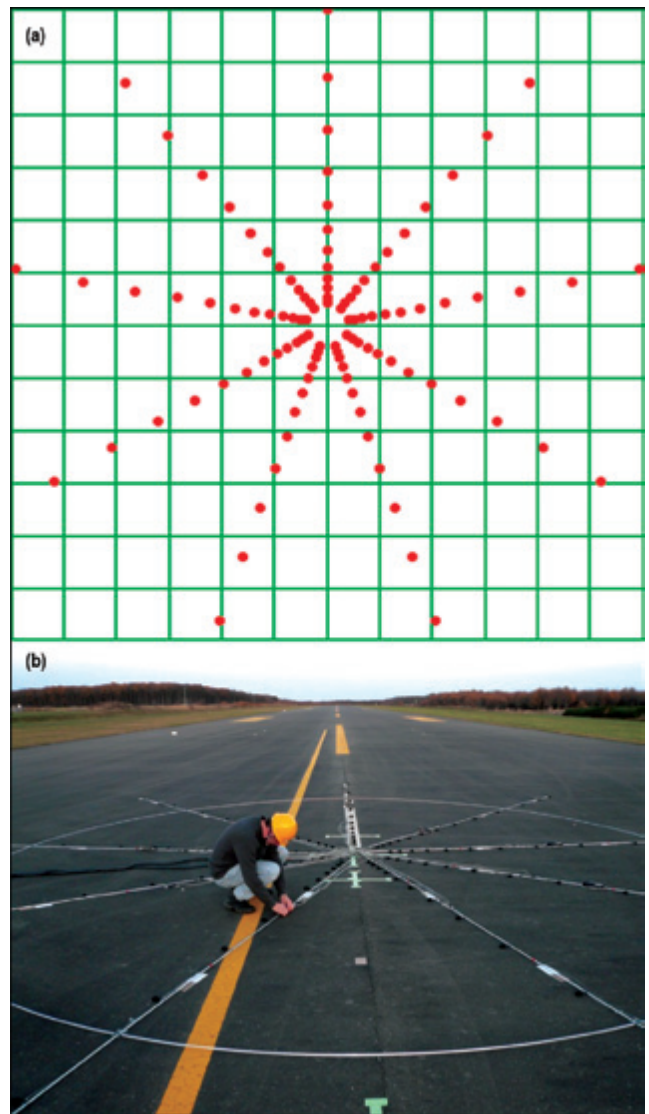


Figure 12. Array geometry and photo of the array on the runway; array diameter is 12 meters, and there are nine radial line arrays each with 12 microphones (108 total microphones).

achieved through the combination of shading and de-convolution. For this illustration, a level flight was chosen with engine idle and the aircraft in landing configuration. Altitude for this measurement was 59 m, and the speed was 57 m/s (≈ 205 km/h).

Figure 13 shows results for the 1-kHz octave band averaged over a 15 m interval and centered where the nose of the aircraft is 5 m past the array center. The resulting FFT spectra were synthesized into full octave bands. The displayed dynamic range is 20 dB, corresponding to a 2-dB level difference between the colors.

Figure 13a shows the DAS map obtained without shading, meaning that resolution will be poor due to the concentration of microphones near the array center. Use of the shading function improves resolution considerably, as shown in Figure 13b. But it also amplifies the side lobes due to the large microphone spacing across the outer part of the active subarray, where each microphone is also given a large weight. Fortunately, the de-convolution process is able to significantly reduce these side lobes, as can be seen in Figure 13c. Better side lobe suppression could have been achieved in DAS by the use of more optimized irregular array geometries (multispiral, for example), but in this work, the focus has been on the ease of array deployment, and de-convolution seems to compensate quite well. The fly-over measurements were made in cooperation with Japan Aerospace Exploration Agency (JAXA).

Summary and Conclusions

This article illustrates how additional de-convolution algorithms can be applied to traditional delay-and-sum measurements and cal-

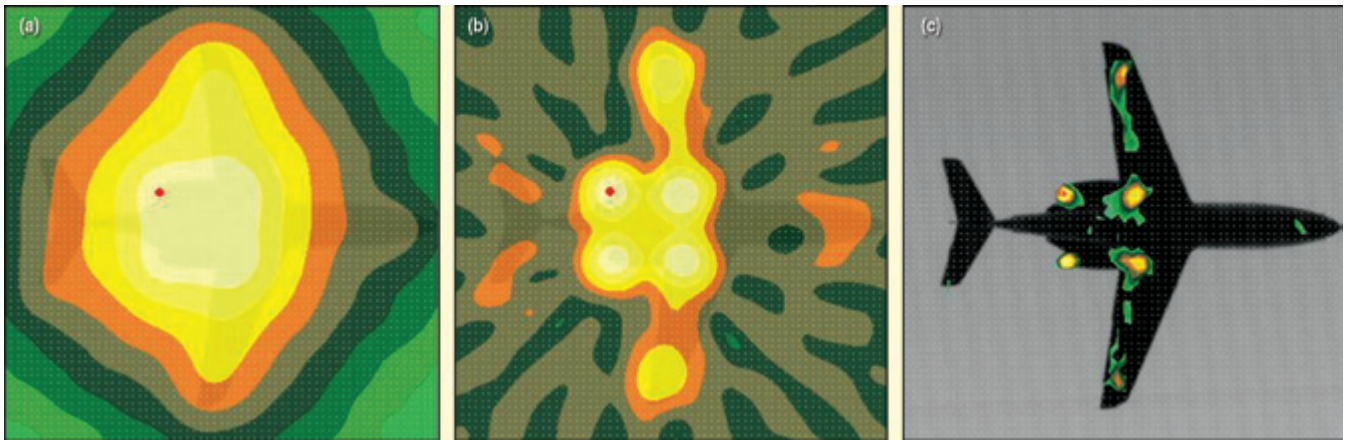



Figure 13. Illustration of the improvements in resolution and dynamic range obtained through the use of shading and de-convolution; data are from a level flight with engine idle and the aircraft in landing configuration; display dynamic range is 20 dB, corresponding to 2-dB contour interval.

culations for noise source identification. This means users can add these algorithms to their existing measurements. The algorithms are efficient and fast FFT-based NNLS (non-negative least squares) and DAMAS2 (de-convolution approach for mapping acoustic sources, Version 2). These improved algorithms using iterative de-convolution techniques offer up to 10 times better resolution. The principle behind these techniques has been described along with measurement examples from the automotive, wind turbine and aerospace industries. The techniques provide considerable improvements in both spatial resolution and in suppression of side lobe effects.

References

1. J. Hald and J. J. Christensen, "A Novel Beamformer Design for Noise Source Location from Intermediate Measurement Distances," *Proceedings of ASA/IFA/MIA*, 2002.
2. J. J. Christensen and J. Hald, "Beamforming," *Brüel & Kjær Technical Re-*

view No. 1, pp. 1–48, 2004, <http://www.bksv.com/Library/Technical%20Reviews.aspx?year=2004-2000&st=2004-2000>.

3. J. Hald, "Combined NAH and Beamforming Using the Same Array–SONAH," *Brüel & Kjær Technical Review No. 1*, pp. 11–50, 2005, <http://www.bksv.com/Library/Technical%20Reviews.aspx?year=2012-2005&st=2012-2005>.
4. Klaus Ehrenfried and Lars Koop, "A Comparison of Iterative De-Convolution algorithms for the Mapping of Acoustic Sources," *American Institute of Aeronautics and Astronautics, AIAA Journal*, Volume 45, No. 7, pp. 1584-1595, 2007.
5. Bernard Ginn and Jørgen Hald "Aerodynamic Noise Source Identification in Wind Tunnels Using Acoustical Array Techniques" *8th MIRA International Vehicle Aerodynamics Conference - 'Low Carbon Vehicles'*, 2010.
6. Jørgen Hald, Yukata Ishii (B&K) and Ishii, Oinuma, Nagai, Yokogawa, Yamamoto (JAXA), "High-resolution Fly-over Beamforming Using a Small Practical Array," *American Institute of Aeronautics and Astronautics, AIAA Journal* (2012) and *Brüel & Kjær Technical Review No. 1, BV 0064-11*, 2012. 

The author may be reached at: svend.gade@bksv.com.